A Damage Sensor Associated with the Cuticle Coordinates Three Core Environmental Stress Responses in *Caenorhabditis elegans*

William Dodd,*,[1] Lanlan Tang,*,[1] Jean-Christophe Lone,[†] Keon Wimberly,* Cheng-Wei Wu,*
Claudia Consalvo,* Joni E. Wright,* Nathalie Pujol,[†,2] and Keith P. Choe*,[2]

*Department of Biology, University of Florida, Gainesville, Florida 32611 and [†]Aix Marseille University, CNRS, INSERM, CIML, Marseille, France

ORCID ID: 0000-0001-8889-3197 (N.P.)

ABSTRACT Extracellular matrix barriers and inducible cytoprotective genes form successive lines of defense against chemical and microbial environmental stressors. The barrier in nematodes is a collagenous extracellular matrix called the cuticle. In *Caenorhabditis elegans*, disruption of some cuticle collagen genes activates osmolyte and antimicrobial response genes. Physical damage to the epidermis also activates antimicrobial responses. Here, we assayed the effect of knocking down genes required for cuticle and epidermal integrity on diverse cellular stress responses. We found that disruption of specific bands of collagen, called annular furrows, coactivates detoxification, hyperosmotic, and antimicrobial response genes, but not other stress responses. Disruption of other cuticle structures and epidermal integrity does not have the same effect. Several transcription factors act downstream of furrow loss. SKN-1/Nrf and ELT-3/GATA are required for detoxification, SKN-1/Nrf is partially required for the osmolyte response, and STA-2/Stat and ELT-3/GATA for antimicrobial gene expression. Our results are consistent with a cuticle-associated damage sensor that coordinates detoxification, hyperosmotic, and antimicrobial responses through overlapping, but distinct, downstream signaling.

KEYWORDS damage sensor; collagen; detoxification; osmotic stress; antimicrobial response

EXTRACELLULAR matrices (ECMs) are ubiquitous features of animal tissues composed of secreted fibrous proteins and polysaccharides. Although they were once considered inert mechanical scaffolds (Hay 1981), it is now clear that there is dynamic and reciprocal cross talk between cells and ECMs that regulates cell differentiation, morphogenesis, and tumorigenesis (Rozario and DeSimone 2010; Clause and Barker 2013; Samarakoon *et al.* 2013; Winograd-Katz *et al.* 2014; Gaggar and Weathington 2016). Less is known about how ECMs influence cellular responses to environmental stress.

Internal and epidermal tissues secrete ECMs as mechanical support. Epidermal ECMs also function as barriers to environmental stress. Examples include a keratin- and lipid-rich matrix in mammals (*i.e.*, the stratum corneum of the skin) and a rigid chitinous exoskeleton in insects. Nematodes such as *Caenorhabditis elegans* are covered by a flexible cuticle of cross-linked collagen fibers that is secreted by underlying epidermal cells (Page and Johnstone 2007; Chisholm and Xu 2012). It provides a first line of defense against desiccation, as well as some pathogens and toxins (Alvarez *et al.* 2007; Partridge *et al.* 2008; Burns *et al.* 2010).

C. elegans mounts distinct cellular responses to stressors that are broadly conserved (Lamitina *et al.* 2006; Wheeler and Thomas 2006; Pujol *et al.* 2008a,b; Rohlfing *et al.* 2011; Choe 2013; Zugasti *et al.* 2014). In response to high osmolarity, *C. elegans* synthesizes the organic osmolyte glycerol in part by inducing *gpdh-1*, which encodes the rate-limiting enzyme GPDH (glycerol-3-phosphate dehydrogenase) (Lamitina *et al.* 2004, 2006). High osmolarity and infection with fungal pathogens that pierce the *C. elegans* cuticle

induce several antimicrobial peptide genes including *nlp-29* (Pujol *et al.* 2008a,b; Zugasti *et al.* 2014). Genetic studies have identified cuticle collagens that are required to regulate *gpdh-1* and *nlp-29* under basal conditions (Lamitina *et al.* 2006; Wheeler and Thomas 2006; Pujol *et al.* 2008b; Choe 2013; Zugasti *et al.* 2016) suggesting that the cuticle may contain a sensor for stress (Lamitina *et al.* 2006; Wheeler and Thomas 2006; Choe 2013; Taffoni and Pujol 2015). The nature of this putative sensor and downstream signaling mechanisms remain poorly defined and it is unclear if other stress responses are also activated.

In response to reactive small molecules, cap "n" collar (CNC) transcription factors activate antioxidant and detoxification genes in nematodes, insects, and mammals (Hu *et al.* 2006; Oliveira *et al.* 2009; Park *et al.* 2009; Sykiotis and Bohmann 2010; Choe *et al.* 2012; Blackwell *et al.* 2015). The single *C. elegans* CNC, SKN-1, promotes stress resistance, slows aging, and extends life span, while the mammalian CNC Nrf2 protects against cancer, neurodegeneration, inflammation, and fibrosis (Oliveira *et al.* 2009; Park *et al.* 2009; Sykiotis and Bohmann 2010). CNCs are regulated by a complex set of intracellular signals that influence posttranslational modifications, degradation, and nuclear translocation (Bryan *et al.* 2013; Niture *et al.* 2013; Blackwell *et al.* 2015); regulation of CNCs via the ECM would represent a distinct mechanism.

We used RNA interference (RNAi) to test disruption of diverse aspects of cuticle and epidermal integrity for activation of six conserved stress responses. Our results show that osmolyte accumulation and detoxification responses are coactivated by disruption of a specific cuticle structure called the annular furrow, and not by general changes in body shape or epidermal integrity. Antimicrobial response genes were also activated by furrow disruption, and more generally by loss of epidermal integrity. Hyperosmolarity also induces *skn-1*-dependent detoxification genes. Surprisingly, we also find that in furrow mutants, *skn-1* is required for full induction of genes that regulate the accumulation of osmolytes. Alternatively, activation of antimicrobial genes by furrow loss is dependent on STA-2/STAT and ELT-3/GATA transcription factors. Our results are consistent with the presence of a damage sensor residing in, or associated with, furrows in the cuticle that coregulates three different stress defense pathways.

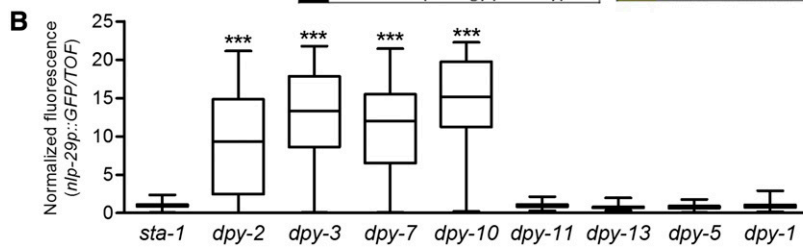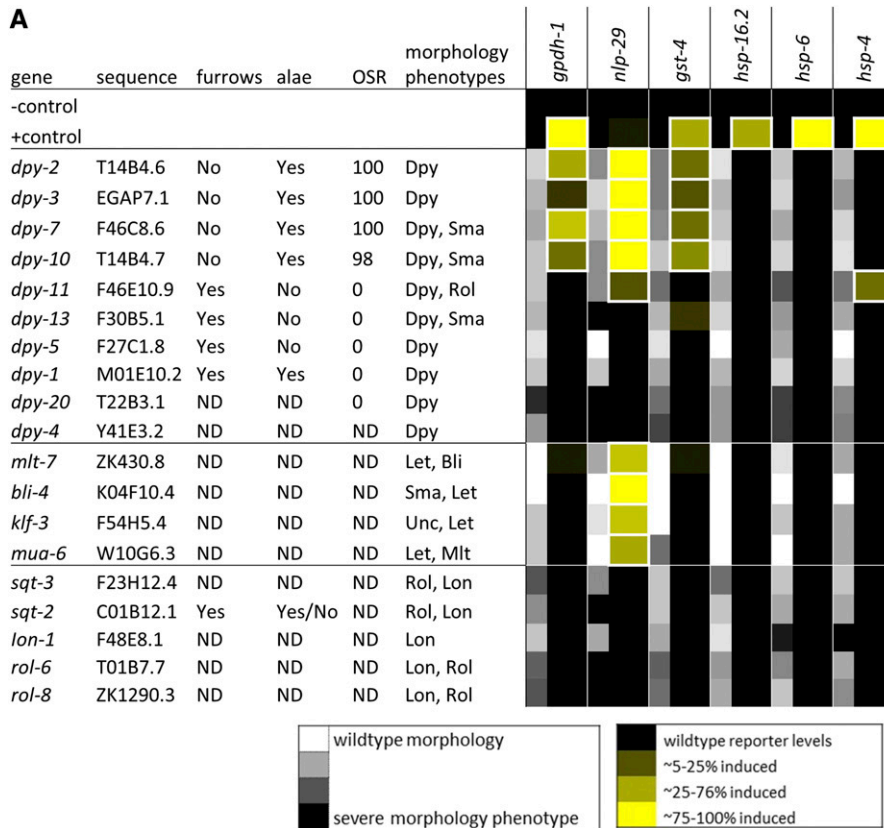## Materials and Methods

C. elegans strains

The following strains were used *vs.*: wild-type N2 Bristol, VP596 *vsIs33*[*dop-3p*::DsRed2];*dvIs19*[*gst-4p*::*GFP*], VP604 *kbIs24* [*gpdh-1p*::DsRed2;*myo-2p*::GFP;*unc-119* rescue], SJ4005 *zcIS4*[*hsp-4p*::GFP], SJ4100 *zcIs13*[*hsp-6p*::GFP], QV65 *gpIs1*[*hsp-16.2p*::GFP];*vsls33*[*dop-3p*::DsRed2], QV285 *frIs7* [*nlp-29p*::GFP, *col-12p*::DsRed], IG274 *frIs7*, CB128 *dpy-10*(*e128*), CB88 *dpy-7*(*e88*), BE3 *sqt-2*(*sc3*), CB61 *dpy-5*(*e61*), QV41 *dpy-10*(*e128*);*vsls33*;*dvIs19*, QV248 *dpy-7*(*e88*);*dvIs19*, QV261

dpy-7(*e88*);*kbIs24*, IG1689 *dpy-7*(*e88*);*frIs7*, IG1710 *dpy-7*(*e88*); *elt-3*(*gk121*);*frIs7*, IG1705 *dpy-7*(*e88*);*sta-2*(*ok1860*);*frIs7*, IG1685 *dpy-3*(*e27*);*frIs7*, G1709 *dpy-3*(*e27*)*elt-3*(*gk121*);*frIs7*, IG1704 *dpy-3*(*e27*);*sta-2*(*ok1860*);*frIs7*, IG1457 *dpy-10*(*e128*); *frIs7*, IG1712 *dpy-10*(*e128*);*elt-3*(*gk121*);*frIs7*, IG1707 *dpy-10*(*e128*);*sta-2*(*ok1860*);*frIs7*, TP12 *kaIs12*[COL-19::GFP], VP332 *gpdh-1*(*kb24*);*gpdh-2*(*kb33*), LD001 *ldIs7*[*skn-1B/C*::GFP + pRF4(*rol-6*(*su1006*))], and GR2245 *skn-1*(*mg570*). QV251, which contains a reporter for gst-10p, was generated using PCR to fuse 951-bp upstream from the start codon to GFP (Hobert 2002). The fusion PCR product was then injected at ~20 ng/µl with *myo-3p*::dsRed as a comarker. Unless noted otherwise, worms were cultured at 20° using standard methods (Brenner 1974).

RNAi and screening

RNAi was performed by feeding worms strains of *Escherichia coli* [HT115(DE3)] that are engineered to transcribe double-stranded RNA (dsRNA) homologous to a target gene (Kamath *et al.* 2001). The cuticle and epidermal screen in Figure 1A was performed with dsRNA feeding constructs from the ORFeome library (Open Biosystems, Huntsville, AL) (Rual *et al.* 2004) and supplemented with clones for *dpy-10*, *dpy-20*, *dpy-3*, and *mua-6* from the genomic library (Geneservice, Cambridge, UK) (Kamath *et al.* 2003). All clones used in Figure 1B were derived from the genomic library. Positive hit clone inserts were verified by sequencing and targets identified using Clone Mapper (Thakur *et al.* 2014). Bacteria with plasmid pPD129.36 expressing 202 bases of dsRNA that are not homologous to any predicted *C. elegans* gene and the *sta-1*(*RNAi*) clone (Zugasti *et al.* 2016) were used as controls for nonspecific RNAi effects. RNAi was performed as described previously (Choe *et al.* 2009) with minor modifications. dsRNA-producing bacteria were grown in lysogeny broth containing selective antibiotic and then transferred to agar nematode growth medium (NGM) plates containing 0.2% β-lactose, or 1 or 3 mM IPTG (Choe *et al.* 2009). Eggs or synchronized populations of L1 larvae were placed on RNAi plates and tested at the young and gravid adult stages.

For the screen in Figure 1A, each dsRNA clone was tested with all six stress response reporter strains in 12-well agar plates in three independent trials. Fluorescent reporter induction was scored manually as an estimate of percent penetrance (0, similar to control vector; 1, ~5–25%; 2, ~25–75%; and 3, ~75% or more) and averaged together across trials for each reporter strain. The penetrance of phenotypes affecting body morphology and behavior was scored on a scale of 0–3 (0, similar to control vector; 1, ~5–10%; 2, ~10–50%; and 3, ~50–100%) and averaged together across all trials with all reporter strains. In all trials except the first, Dumpy was also scored for expressivity (0, similar to control vector; 1, mild; 2, moderate; and 3, strong Dumpy), and the penetrance and expressivity scores were averaged together to calculate an average value for the strength of the morphology phenotype. Only results for clones that caused an average morphology phenotype score of ≥ 1.0 are shown.

A

gene	sequence	furrows	alae	OSR	morphology phenotypes	gpdh-1	nlp-29	gst-4	hsp-16.2	hsp-6	hsp-4
-control											
+control											
dpy-2	T14B4.6	No	Yes	100	Dpy						
dpy-3	EGAP7.1	No	Yes	100	Dpy						
dpy-7	F46C8.6	No	Yes	100	Dpy, Sma						
dpy-10	T14B4.7	No	Yes	98	Dpy, Sma						
dpy-11	F46E10.9	Yes	No	0	Dpy, Rol						
dpy-13	F30B5.1	Yes	No	0	Dpy, Sma						
dpy-5	F27C1.8	Yes	No	0	Dpy						
dpy-1	M01E10.2	Yes	Yes	0	Dpy						
dpy-20	T22B3.1	ND	ND	0	Dpy						
dpy-4	Y41E3.2	ND	ND	ND	Dpy						
mlt-7	ZK430.8	ND	ND	ND	Let, Bli						
bli-4	K04F10.4	ND	ND	ND	Sma, Let						
klf-3	F54H5.4	ND	ND	ND	Unc, Let						
mua-6	W10G6.3	ND	ND	ND	Let, Mlt						
sqt-3	F23H12.4	ND	ND	ND	Rol, Lon						
sqt-2	C01B12.1	Yes	Yes/No	ND	Rol, Lon						
lon-1	F48E8.1	ND	ND	ND	Lon						
rol-6	T01B7.7	ND	ND	ND	Lon, Rol						
rol-8	ZK1290.3	ND	ND	ND	Lon, Rol						

Legend (morphology): wildtype morphology → severe morphology phenotype.
Legend (reporter levels): wildtype reporter levels, ~5-25% induced, ~25-76% induced, ~75-100% induced.

B Box plot: Normalized fluorescence (*nlp-29p::GFP*/TOF), values 0–25, for *sta-1*, *dpy-2*, *dpy-3*, *dpy-7*, *dpy-10*, *dpy-11*, *dpy-13*, *dpy-5*, *dpy-1*. *** above *dpy-2*, *dpy-3*, *dpy-7*, *dpy-10*.

Figure 1 Genetic disruption of specific *dpy* genes activates detoxification, antimicrobial, and osmotic stress responses. (A) Double-stranded RNA (dsRNA)-expressing clones for genes required for diverse aspects of cuticle and epidermal integrity were scored for cuticle and morphology phenotypes and induction of stress response reporters. Stress response reporters were scored for penetrance and averaged together across three trials. Cuticle and morphology phenotype penetrance and expressivity (Dpy only) were scored and averaged together across three trials for each reporter line. Positive controls for reporters were 200 mM NaCl for *gpdh-1* and *nlp-29*, *wdr-23*(RNAi) for *gst-4*, 34° for 1 hr for *hsp-16.2*, 0.5 mM paraquat for *hsp-6*, and 10 μg/ml tunicamycin for *hsp-4*. ND, not determined. Reporter results outlined with a thick white boarder were positive in at least two of three trials. Percent acute osmotic stress resistance (OSR) from trial run in (B) and the presence (Yes) or absence (No) of intact furrows and alae (from Figure 2) are also summarized. (B) The ratio of *nlp-29p*::GFP to time of flight was measured in a BIOSORT and normalized to the negative control *sta-1*(RNAi). n = 99–228 worms. Boxes are 25% percentiles above and below the median, and whiskers are minimum and maximum.

Quantitative PCR and transgene analysis

Detoxification gene reporters (*gst-4p*::*GFP* and *gst-10p*::*GFP*) and COL-19::GFP were imaged with an Olympus BX60 microscope with UPlanFl objectives and a Zeiss Axiocam MRm camera ([Carl Zeiss], Thornwood, NY). Fluorescence of *nlp-29p*::*GFP* was quantified using a COPAS BIOSORT as previously described (Pujol *et al.* 2008a) and normalized to time of flight. The BIOSORT was not sensitive enough to reliably measure *gst-4p*::*GFP* and *gpdh-1p*::*dsRed2* fluorescence in *dpy-7* worms and these were instead quantified manually in individual worms from images using Image J 1.48v to calculate average whole-worm fluorescence. Hypodermal-specific *gst-4p*::*GFP* fluorescence was also scored manually in individual worms as follows: low (dim signal limited to a few spots), medium (dim signal throughout the epidermis or bright signal only in head or tail regions), and high (bright signal throughout the epidermis). In one experiment, *gst-4p*::*GFP* was quantified using a fluorescent plate reader (Synergy HT; BioTek) (Leung *et al.* 2011). SKN-1b/c::GFP was visualized with a Zeiss Axiovert 200M inverted microscope, and an LCM 5 Pascal Vario One confocal laser scanning system and 40× C-apochromat water objective.

Quantitative PCR (qPCR) assays were performed by isolating total RNA with a Quick-RNA MicroPrep kit from ZYMO Research. Reverse transcription and PCR were performed with the GoTaq 2-Step RT-qPCR system from Promega in an Eppendorf RealPlex2 using primers for *rpl-2* or *cdc-42* as internal controls. Relative mRNA levels were calculated using the ΔΔCT method adjusted with primer efficiencies calculated from standard curves. Primer sequences are provided in Supplemental Material, Table S1.

Whole-transcriptome RNA sequencing

N2 worms were synchronized at the L1 larval stage via hypochlorite treatment and grown on RNAi bacteria. For high NaCl, N2 worms were transferred to 300 mM NaCl NGM agar plates as young adults and exposed for 3 or 24 hr. Mutant *dpy-7* worms were harvested 1 day after first becoming gravid, which corresponds to when osmotic and detoxification gene reporters are most active. RNA was extracted from three replicates per treatment, with ~1000–2000 worms per replicate,

using the RNAqueous-Micro Total RNA Isolation Kit (ThermoFisher Scientific). Total RNA was sent to The Yale Center for Genome Analysis for 75 nucleotide single-end sequencing in an Illumina HiSequation 2000.

Raw sequences were processed with Kallisto to quantify transcripts and Sleuth was used for differential abundance analysis (Pimentel *et al.* 2017), which generated an estimate for differential gene expression effect size termed "b" that is analogous to $\log_2$ fold change and an adjusted *P*-value termed "q." We analyzed six pairs of conditions from our experiment and a previously published pair of raw sequence data (GSE63075) (Steinbaugh *et al.* 2015).

We considered genes differentially expressed if they had a *q*-value $\leq$ 0.05 and a *b*-value $\geq$ 1 or $\leq$ −1. All differentially expressed genes present in all conditions were clustered with Gene Cluster 3.0 using correlation (uncentered) average linkage and mapped with Java Treeview 1.1.6r4. Differentially expressed genes were tested for Gene Ontology analysis by DAVID (the Database for Annotation, Visualization, and Integrated Discovery) 6.8 for gene functional classification using a high stringency (Huang *et al.* 2009); classifications with a Benjamini adjusted $P \leq 0.05$ are listed.

In vivo assays

Acute osmotic resistance assays were performed by counting the percentage of worms that responded to gentle touches with a worm pick after 10 min on an agar plate with 500 mM NaCl, as described previously (Wheeler and Thomas 2006). Longevity and juglone resistance assays were performed as described previously (Tang and Choe 2015), except that instead of using floxuridine (FUDR) for longevity studies on high NaCl, adults were manually transferred to fresh plates daily for the first few days to avoid mixing generations. Osmotic survival assays were performed by transferring worms from 51 to 450 mM NaCl agar plates and counting live and dead worms a day later.

Glycerol assays

Glycerol assays were conducted on populations of whole worms lysed by sonication using the PicoProbe Free Glycerol Fluorometric Assay Kit (Biovision). Values were normalized to total protein using the Pierce BCA Protein Assay Kit (ThermoFisher Scientific).

Statistical analysis

Statistical significance was determined using a Student's *t*-test when two means were compared, a one-way ANOVA with a Dunnet or Tukey's *post hoc* test when three or more means were compared, a log-rank test when survival curves were compared, and a χ^2 test for categorical reporter data. Overall *P*-values of < 0.05 were taken to indicate statistical significance. Bonferroni corrections to *P*-values were used when more than two survival curves were compared.

Data availability

Strains are available upon request. Raw numeric data are at https://figshare.com/s/7863ed7b6e2bed9e6510 and RNAseq (RNA sequencing) raw data are at the Gene Expression Omnibus (GSE107704).

Results

RNAi screening identifies a specific cuticle structure required for regulation of detoxification, osmolyte, and antimicrobial responses

The cuticle is a complex ECM composed of over 100 distinct collagen proteins secreted from underlying epidermal cells. It forms a hydrostatic skeleton, and acts as the primary barrier and first line of defense against many environmental insults (Johnstone 2000; Alvarez *et al.* 2007; Burns *et al.* 2010). The cuticle is composed of multiple layers, some with distinct structures discernable by light and/or electron microscopy. We used dsRNA feeding to disrupt diverse aspects of cuticle or epidermal integrity and test for induction of six stress response gene reporters: osmolyte accumulation (*gpdh-1*), antimicrobial (*nlp-29*), detoxification (*gst-4*), heat shock (*hsp-16.2*), and mitochondrial and endoplasmic reticulum unfolded protein (*hsp-6* and *hsp-4*, respectively). These stress responses are conserved and well studied in *C. elegans* (Jones *et al.* 1989; Shen *et al.* 2001; Yoneda *et al.* 2004; Lamitina *et al.* 2006; Pujol *et al.* 2008a).

Morphology phenotypes and reporter scores averaged over three trials are shown in Figure 1A, organized by morphology phenotype and strength of reporter induction. Results for the 19 of 40 dsRNA feeding clones that caused the most consistent morphology phenotypes are shown (gray shading), with variation between trials as is common with feeding clones (Zugasti *et al.* 2016). A test was considered positive if the reporter gene was induced in $\geq$ 5% of the worm population, in at least two of three trials (white outlined boxes). We report for the first time that silencing of four cuticle/epidermal integrity genes activates *gst-4p*::*GFP*, as well as *gpdh-1p*::*DsRed2* and *nlp-29p*::*GFP*. We also observed acute osmotic stress resistance when silencing the same genes (Figure 1A, Figure S1A in File S1, and Table S2), a phenotype associated with *gpdh-1* induction (Wheeler and Thomas 2006). The *hsp-16.2* and *hsp-6* reporters were not activated by any clones. Silencing of many other genes caused a diverse range of expected cuticle, morphology, and epidermal phenotypes (*e.g.*, Dumpy, Blister, Roller, Long, and Molting defect), but did not consistently activate *gst-4* or *gpdh-1* reporters. Together, these results suggest that detoxification and osmolyte responses are activated by silencing of a specific subset of *dpy* collagens and not by body shape or general epidermis disorganization. Consistent with previous studies (Tong *et al.* 2009; Ward *et al.* 2014; Taffoni and Pujol 2015; Zugasti *et al.* 2016), the *nlp-29* reporter was activated by silencing the same specific *dpy* genes, but was also activated by loss of genes that cause severe disruption of molting or epidermal integrity (*mlt-7*, *bli-4*, *klf-3*, and *mua-6*) and slightly by loss of *dpy-11*, which also activated *hsp-4*.

We also used a COPAS BIOSORT to quantify *nlp-29p*::*GFP* fluorescence with RNAi inactivation of 11 *dpy* genes (Figure 1B and Figure S1 in File S1), nine of which overlap with Figure 1A. These results confirmed strong activation of *nlp-*
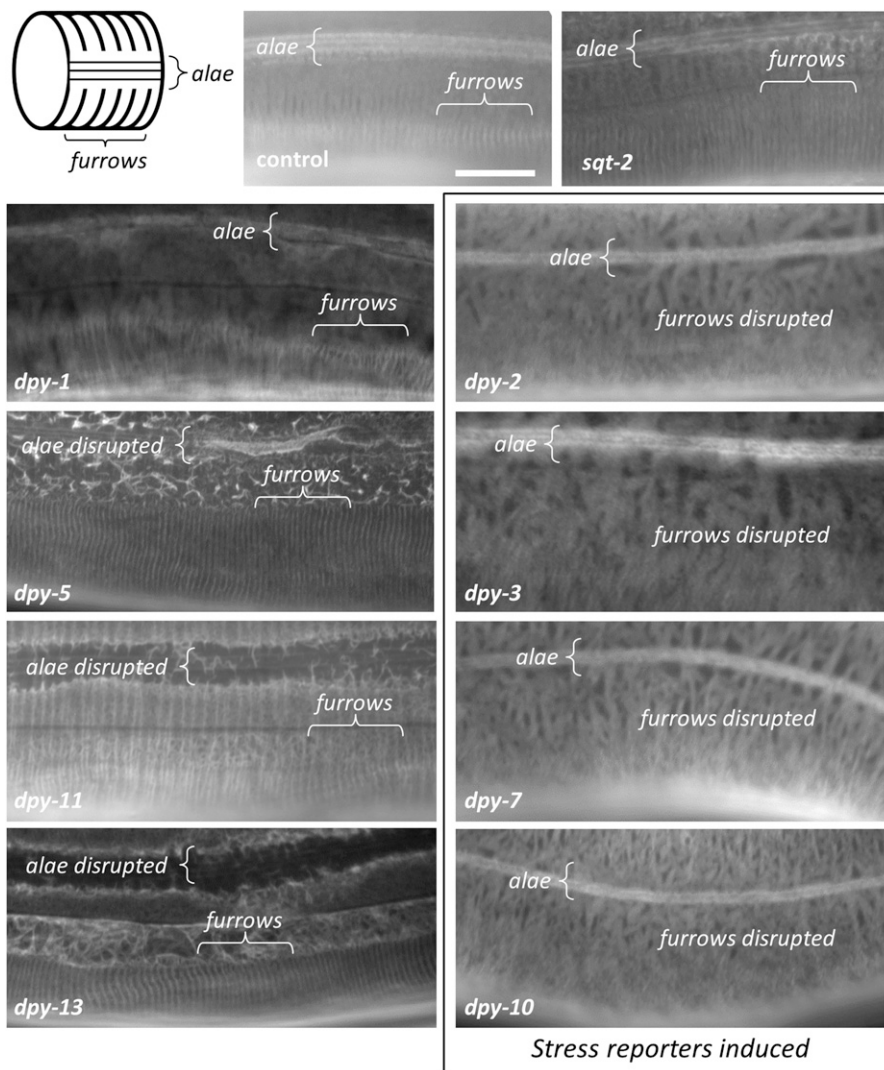
Figure 2 The cuticle furrow is disrupted by *dpy* double-stranded RNA clones that activate stress responses. A model of cortical cuticle structures and fluorescent micrographs of COL-19::GFP in worms treated with RNA interference. Images are representative of 10 worms. Bar, 10 μM.

29p::*GFP* with *dpy-2*, *3*, *7*, and *10* and lack of strong activation with *dpy-11*, *13*, *5*, *1*, and *20*; they also added *dpy-8* and *9* to the list of *dpy* clones activating *nlp-29p*::*GFP*. *nlp-29p*::*GFP* induction has also been confirmed in mutants of *dpy-9* and *10* (Pujol *et al.* 2008b; Zugasti *et al.* 2014). Interestingly, mutants of *dpy-2*, *3*, *7*, *8*, *9*, and *10* were previously found to have no annular furrows but did have other cuticle structures including alae, which are lateral ridges in the cuticle perpendicular to furrows (Cox *et al.* 1980; McMahon *et al.* 2003; Thein *et al.* 2003); morphology and stress response results are summarized for *dpy* genes in Table S2.

To confirm the role of alae and furrows, we silenced *dpy-2*, *3*, *7*, and *10*, and five other collagens with morphology phenotypes (*dpy-5*, *11*, *1*, *13*, and *sqt-2*), in a strain of worm expressing COL-19::GFP, a collagen marker that labels the matrix of the circumferential transverse annuli and the trilaminate lateral alae (Thein *et al.* 2003). Similar to prior analysis of mutants, silencing of *dpy-2*, *3*, *7*, or *10* completely disrupted the wild-type parallel pattern of furrows without eliminating alae (Figure 2). Conversely, silencing of *dpy-5* or *13* eliminated alae without disrupting furrows, and silencing

of *dpy-1* and *sqt-2* did not cause any obvious disruption to either alae or furrows.

Silencing *dpy-11* caused partial irregular branching of furrows and eliminated alae. Interestingly, it was only with *dpy-11* RNAi that we observed activation of the endoplasmic reticulum stress response reporter (*hsp-4*) together with weak activation of the antimicrobial reporter (*nlp-29*) (positive in two out of three visual scoring trials and a nonsignificant 1.4-fold increase in BIOSORT quantification). Unlike most of the other Dpy genes tested, *dpy-11* does not encode a collagen but rather a nematode-specific protein with a thioredoxin domain (pfam00085). It is exclusively expressed in epidermal cells, where is has been suggested to be localized to the endoplasmic reticulum or Golgi apparatus (Ko and Chow 2002). It may be required for the maturation of cuticle collagens, but could also be involved in post-translational modification of other substrates, including signaling molecules linked to a distinct cellular stress pathway.

We next used qPCR with two collagen mutants with disrupted furrows [*dpy-10*(*e128*) and *dpy-7*(*e88*)], one with intact furrows [*dpy-5*(*e61*)], and one reported to have more
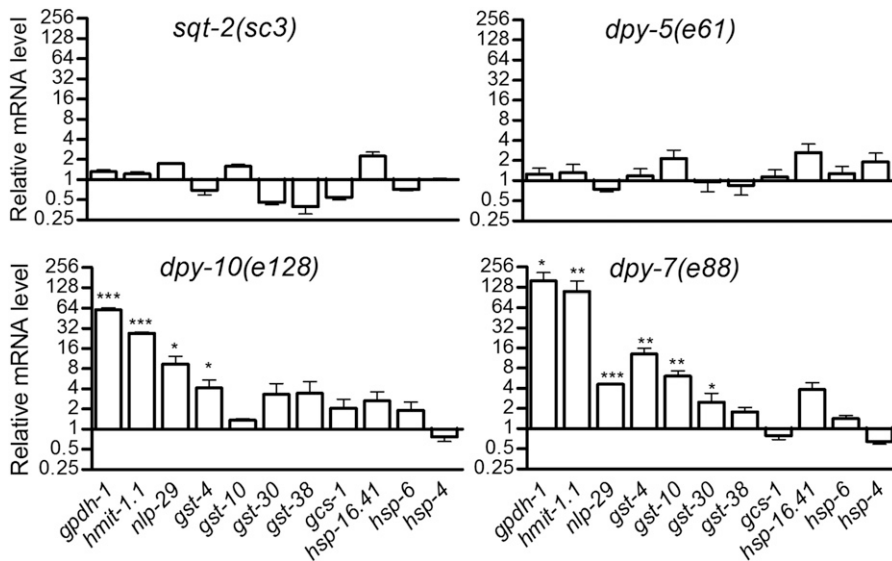
Figure 3 Quantitative PCR verification of stress response gene expression. mRNA levels for stress-inducible genes in four collagen mutants. $n = 3$–9 replicates of worms combined from one or two trials. * $P < 0.05$, ** $P < 0.01$, and *** $P < 0.001$ relative to N2, which was normalized to a mean of 1.0.

general alae and furrow disruption [*sqt-2*(*sc3*)] (Thein *et al.* 2003). As shown in Figure 3, *gpdh-1*, *gst-4*, and *nlp-29* were induced in *dpy-10* and *dpy-7* worms, but not in *sqt-2* or *dpy-5* worms, similar to the RNAi results (Figure 1). Another osmotic response gene (*hmit-1.1*) (Kage-Nakadai *et al.* 2011) was also induced only in *dpy-10* and *dpy-7* worms, and detoxification response genes (*gst-10* and *gst-30*) were induced in *dpy-7* worms. Other stress responsive genes that we tested were not induced by any of the mutations (Figure 3).

Taken together, Figure 1, Figure 2, and Figure 3 suggest that specific loss of annular furrows, and not alteration of body shape, alae, or general epidermal integrity, initiates a signal that coactivates osmolyte accumulation, antimicrobial, and detoxification responses, but not all stress responses. The antimicrobial *nlp-29* reporter also responded to detachment of the cuticle (blister phenotype, *bli-4* and *mlt-7*), hemidesmosome disruption (*mua-6*), disruption of muscle/cuticle attachments (*klf-3*), and disruption of fatty acid metabolism (*acs-3* and *fasn-1*) (Lee *et al.* 2010; Ward *et al.* 2014); the *nlp-29* reporter also responded weakly to loss of thioredoxin domain-encoding gene *dpy-11*. This is consistent with *nlp-29* being activated by a broad range of signals affecting epidermal integrity (Pujol *et al.* 2008a; Zugasti *et al.* 2016).

Given that furrow mutants accumulate high levels of glycerol (Lamitina *et al.* 2006; Wheeler and Thomas 2006), we speculated that detoxification, antimicrobial, and osmolyte accumulation stress responses could be induced in response to high internal osmolarity. As expected, *dpy-7*(*RNAi*) strongly induced glycerol accumulation in wild-type worms (Figure S1B in File S1). Deletions in both *gpdh* genes (*gpdh-1* and *2*) reduced glycerol accumulation by *dpy-7*(*RNAi*) almost completely, *i.e.*, by 87% (Figure S1B in File S1). When measured by qPCR, *dpy-7*(*RNAi*) was able to significantly increase *gst-4*, *nlp-29*, and *hmit-1.1* mRNA levels in *gpdh* knockout worms, albeit by a reduced relative amount compared to wild-type in part because of elevated basal levels (Figure

S1C in File S1). Therefore, loss of furrows can activate stress responses without the majority of glycerol accumulation.

Role of *skn-1* in gene expression during osmotic stress and in *dpy-7* mutants

The transcription factor SKN-1 was previously reported to be important for detoxification responses under basal conditions and during oxidative stress (Oliveira *et al.* 2009; Park *et al.* 2009). We addressed the role of SKN-1 in *dpy-7*(*e88*) mutants and worms exposed to 300 mM NaCl for 3 or 24 hr with RNAseq. We also reanalyzed a previously published RNAseq data set for *skn-1*(*RNAi*) under basal conditions (Steinbaugh *et al.* 2015). Genes upregulated by *dpy-7*(*e88*) or osmotic stress were similar to those from previous studies of *dpy-10* mutants and osmotic stress (Rohlfing *et al.* 2010), and include osmolyte accumulation, pathogen response, and detoxification response (Table S3). As expected, *skn-1*(*RNAi*) reduced expression of many phase II detoxification genes (Table S3).

A heat map of genes differentially expressed in at least one of the seven comparisons and clustered by expression is shown in Figure 4, with a table of correlation coefficients below (values are in Table S4 and Table S5 and Gene Expression Omnibus, GSE107704). The longer 24-hr exposure to 300 mM NaCl had similar effects on expression as *dpy-7*(*e88*) (correlation coefficient of 0.77), and they both upregulated more genes than they downregulated. The shorter 3-hr exposure to 300 mM NaCl had a smaller effect. The cluster of genes upregulated by high NaCl and *dpy-7*(*e88*) is enriched for structural functions (cuticle collagen, nidogen, cadherin, and myosin-like) and detoxification [UGT (glycosyltransferase), cytochrome P450, GST (glutathione *S*-transferase), and ABC transporters, Figure 4]. The cluster of genes downregulated by 300 mM NaCl and *dpy-7*(*e88*) is enriched for cuticle collagen, F-box, and fatty acid metabolism. These data are consistent with gene expression responses to compensate
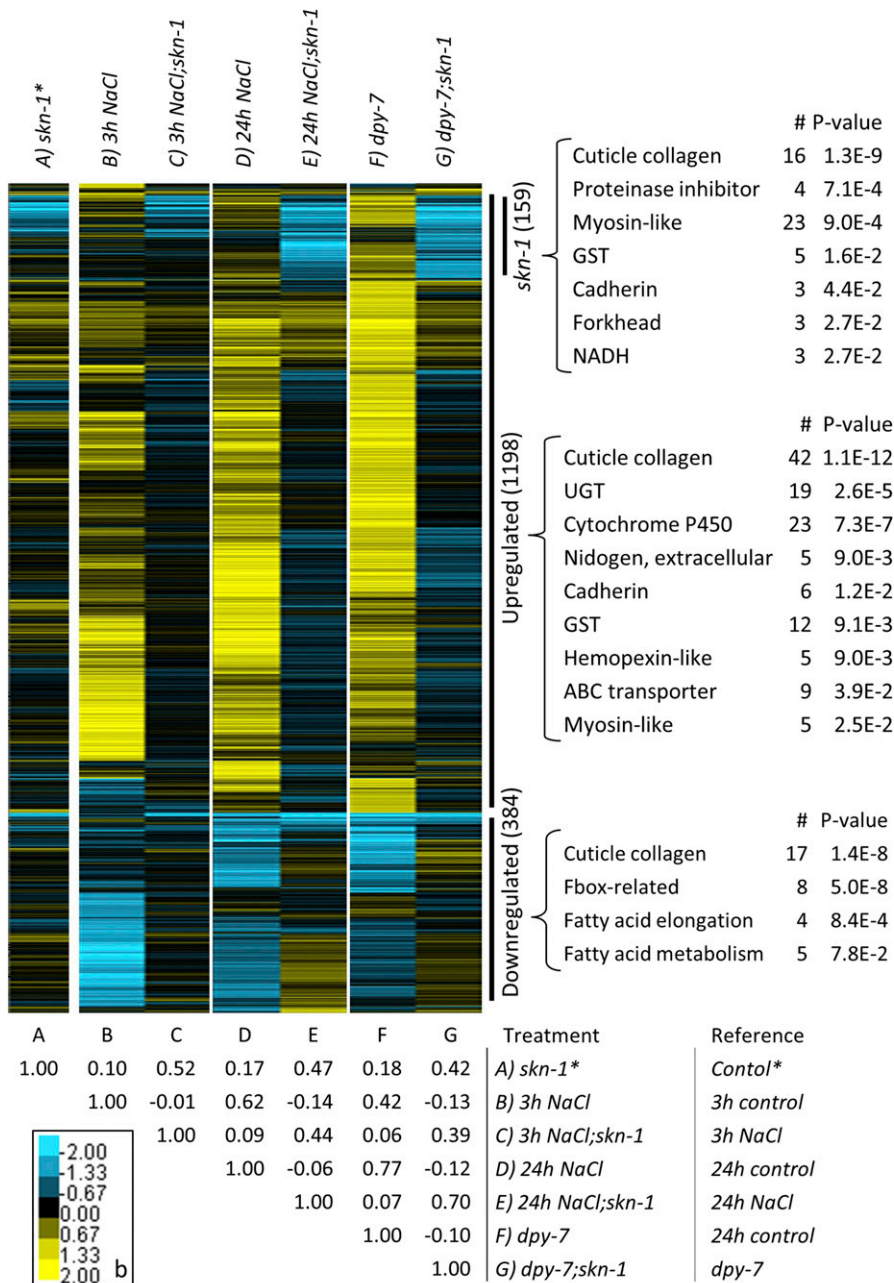
Figure 4 Heat map of differentially expressed genes clustered by relative expression change. All 1594 genes that were differentially expressed in at least one of the seven comparisons and present in all conditions tested are included. Average sleuth analysis estimates of expression effect size for each comparison ("b") are provided on a log$_2$ scale from decreased (blue) to increased (yellow). Correlation coefficients are provided below the heat map. GSE63075 data from N2 with and without *skn-1*(RNAi) (Steinbaugh *et al.* 2015) are included. Gene functional category enrichments are from the Database for Annotation, Visualization, and Integrated Discovery (DAVID) 6.8. *n* = 3 replicates of worms per treatment.

skn-1 (159)

	#	P-value
Cuticle collagen	16	1.3E-9
Proteinase inhibitor	4	7.1E-4
Myosin-like	23	9.0E-4
GST	5	1.6E-2
Cadherin	3	4.4E-2
Forkhead	3	2.7E-2
NADH	3	2.7E-2

Upregulated (1198)

	#	P-value
Cuticle collagen	42	1.1E-12
UGT	19	2.6E-5
Cytochrome P450	23	7.3E-7
Nidogen, extracellular	5	9.0E-3
Cadherin	6	1.2E-2
GST	12	9.1E-3
Hemopexin-like	5	9.0E-3
ABC transporter	9	3.9E-2
Myosin-like	5	2.5E-2

Downregulated (384)

	#	P-value
Cuticle collagen	17	1.4E-8
Fbox-related	8	5.0E-8
Fatty acid elongation	4	8.4E-4
Fatty acid metabolism	5	7.8E-2

| A	B	C	D	E	F	G	Treatment	Reference
1.00	0.10	0.52	0.17	0.47	0.18	0.42	A) *skn-1**	*Contol**
	1.00	-0.01	0.62	-0.14	0.42	-0.13	B) *3h NaCl*	*3h control*
		1.00	0.09	0.44	0.06	0.39	C) *3h NaCl;skn-1*	*3h NaCl*
			1.00	-0.06	0.77	-0.12	D) *24h NaCl*	*24h control*
				1.00	0.07	0.70	E) *24h NaCl;skn-1*	*24h NaCl*
					1.00	-0.10	F) *dpy-7*	*24h control*
						1.00	G) *dpy-7;skn-1*	*dpy-7*

b

*meta-analysis of data from GSE63075

for osmotically-induced mechanical stress and changes to metabolism.

Using our analysis pipeline applied to a previously published data set, *skn-1*(RNAi) only downregulated 20 genes under basal conditions; *skn-1*(RNAi) only downregulated 1.2% of the genes upregulated by 3 hr of 300 mM NaCl (Table S3). Alternatively, *skn-1*(RNAi) downregulated 4.1 and 12.1% of the genes upregulated by 24 hr NaCl and *dpy-7*(e88), respectively. These data indicate that SKN-1 plays a larger role in gene regulation during chronic high NaCl and furrow loss than under basal conditions and short-term high-NaCl exposure. The cluster of genes most strongly downregulated by *skn-1*(RNAi) in the heat map

are enriched for detoxification and structural functions (top of Figure 4), which is similar to enrichment within all genes upregulated by 24-hr 300 mM NaCl and *dpy-7*(e88). It is also clear in the heat map that many genes are induced independently of *skn-1*.

In Figure S2 in File S1, we present Sleuth b and *q*-values for core genes of the six stress responses screened in Figure 1. Similar to the reporter data, *dpy-7* significantly activated genes of the osmotic, antimicrobial, and detoxification responses without activating other stress responses. Exposure to 300 mM NaCl had similar effects, particularly at 24 hr. As expected, *skn-1*(RNAi) reduced induction of many phase II detoxification genes, particularly within the *gst* gene class.
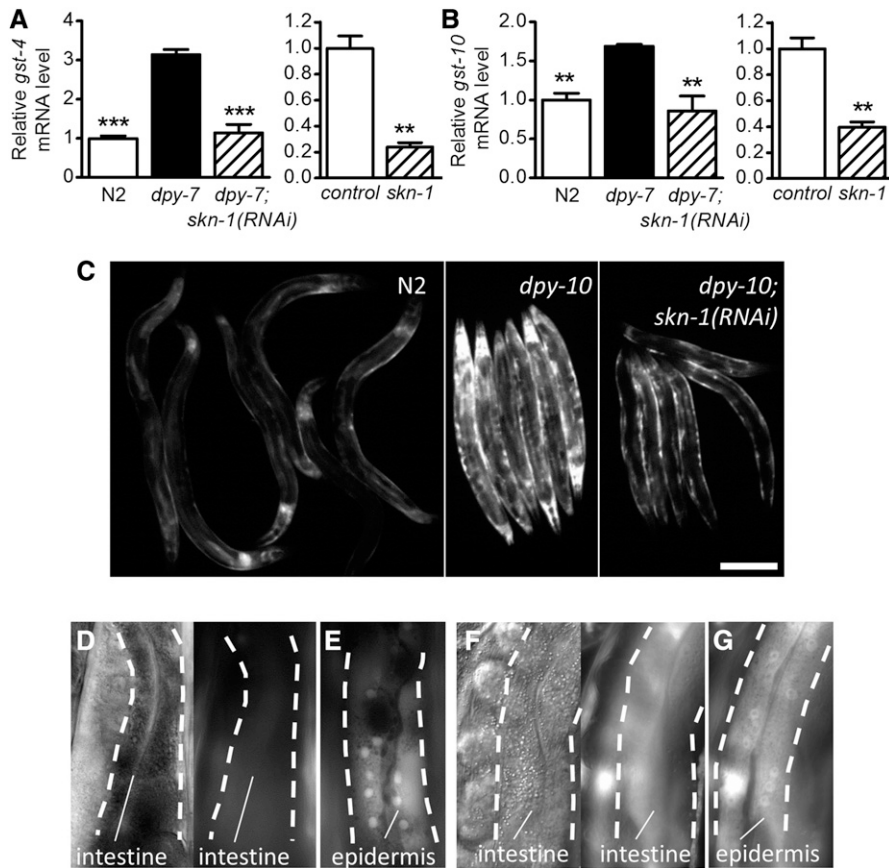
Figure 5 Disruption of cuticle annular furrows activates *skn-1*-dependent detoxification genes in the epidermis. (A and B) mRNA levels for *gst-4* and *gst-10* with and without *skn-1*(*RNAi*) in *dpy-7*(*e88*) worms (left graphs); results for *skn-1*(*RNAi*) in N2 worms are included for reference (right graphs). ** $P < 0.001$ and *** $P < 0.001$ relative to *dpy-7* or control. (C) *gst-4p*::GFP fluorescence images in N2, *dpy-10*(*e128*), and *dpy-10*(*e128*); *skn-1*(*RNAi*) worms. (D and E) *gst-4p*::GFP in *dpy-10*(*e128*) worms; images taken at the focal plane of the intestine are paired with a differential interference contrast micrograph. (F and G) *gst-10p*::GFP in *dpy-7* (*RNAi*) worms; images taken at the focal plane of the intestine are paired with a differential interference contrast micrograph. (D–G) Broken lines mark the boundaries for the intestine (left) or epidermis (right). RNAi, RNA interference.

Surprisingly, expression of *gpdh-1* and *hmit-1.1* osmolyte accumulation genes were partially decreased by *skn-1*(*RNAi*) in *dpy-7*(*e88*). Upregulation of some antimicrobial genes was actually slightly enhanced by *skn-1*(*RNAi*) at 24-hr NaCl and in *dpy-7*(*e88*). Lastly, there were also many *ugt* and a few *gst* genes that were induced regardless of *skn-1*(*RNAi*), suggesting independent or compensatory mechanisms of regulation.

Annular furrow defects activate detoxification genes in the epidermis via SKN-1

Members of the *gst* gene class are well-established targets of SKN-1, and qPCR confirmed the requirement of *skn-1* for expression of *gst-4* and *gst-10* in *dpy-7*(*e88*) worms (Figure 5, A and B); these two direct targets are also under the control of *skn-1* in wild-type worms (Figure 5, A and B). As shown in Figure 5C, a *gst-4p*::GFP reporter was activated in *dpy-10*(*e128*) worms in a *skn-1*-dependent manner. We next used the *gst-4p*::GFP reporter and another SKN-1 target reporter, *gst-10p*::GFP, to identify the tissues in which detoxification genes were induced. In *dpy-10*(*e128*) and *dpy-7*(*RNAi*) worms, *gst-4p*::GFP and *gst-10p*::GFP fluorescence was predominantly visible in epidermal cells (Figure 5, D–G). This contrasts with the robust SKN-1 activation observed in the intestine during oxidative stress (An and Blackwell 2003; Kell *et al.* 2007; Kahn *et al.* 2008; Choe *et al.* 2009). Exposure of *dpy-7*(*e88*) worms to acrylamide, a strong SKN-1 inducer,

activated *gst-4p*::GFP strongly in the intestine (Figure S3B in File S1), indicating that the intestinal detoxification response is still intact when furrows are disrupted.

High external osmolarity activates skn-1-dependent detoxification genes in the epidermis

Given the similar transcriptional profiles observed with high NaCl and *dpy-7*(*e88*) (Figure 4), we next addressed the role of SKN-1 in gene regulation upon osmotic stress. As shown in Figure 6, A and B, high concentrations of NaCl or sorbitol induced *gst-4p*::GFP by a *skn-1*-dependent mechanism. Similar to *dpy-7* and *dpy-10* worms, the reporter was predominantly induced in the epidermis (Figure 6C). qPCR confirmed induction of *gst-4* and another detoxification gene, *ugt-57*, via *skn-1* in worms exposed to 300 mM NaCl for 3 hr (Figure 6, D and E). Using a fluorescent plate reader, we observed induction of *gst-4p*::GFP by as little as 118 mM sorbitol (Figure 6F), a level that has no obvious effects on worm health in our hands.

The *skn* gene generates three different transcripts (*skn-1a*, *b*, and *c*) that share a common C-terminus but with alternative start sites, and our dsRNA clone targets all three. *gst-4* mRNA was fully induced by 300 mM NaCl and *dpy-7*(*RNAi*) in a recently engineered strain with a stop codon introduced into the first *skn-1a*-specific exon (Figure S4A in File S1), consistent with either *skn-1b* or *c* functioning in these contexts. Although some prooxidants and genetic manipulations that induce the expression of *skn-1*-dependent genes provoke
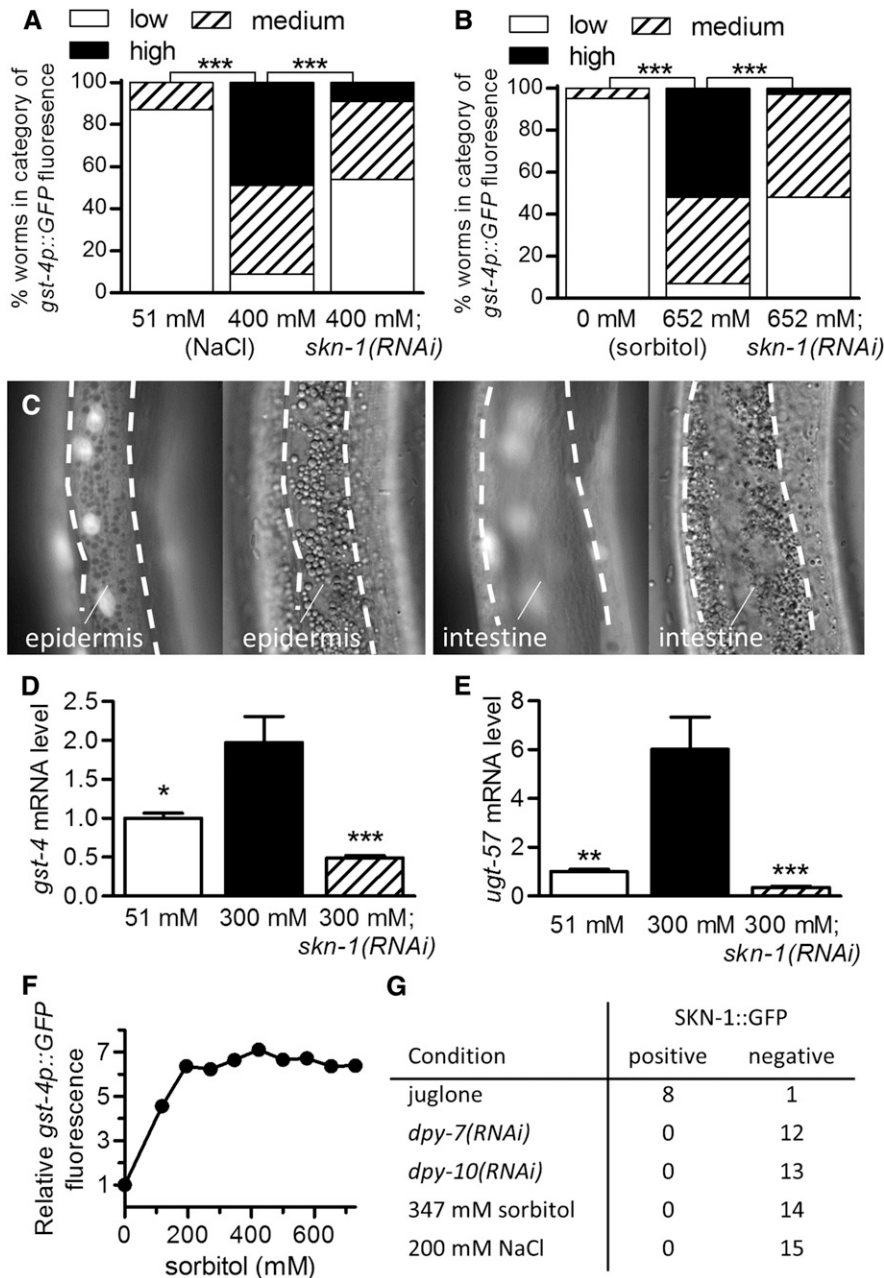
Figure 6 High osmolarity activates *skn-1*-dependent detoxification genes in the epidermis. *gst-4p*::*GFP* is induced in worms exposed to 400 mM NaCl (A) or 652 mM sorbitol (B), and suppressed by *skn-1(RNAi)* (*** $P < 0.001$); low (dim signal limited to a few spots), medium (dim signal throughout the epidermis or bright signal only in head or tail regions), and high (bright signal throughout the epidermis). (C) Paired fluorescent and differential interference contrast images of the intestine (left) and epidermis (right) of a worm exposed to 400 mM NaCl. (D and E) Relative *gst-4* and *ugt-57* mRNA levels in worms exposed to 300 mM NaCl for 3 hr with and without *skn-1(RNAi)* (* $P < 0.05$, ** $P < 0.01$, and *** $P < 0.001$ *vs.* 300 mM, $n = 4$–5 populations of worms). (F) *gst-4p*::*GFP* fluorescence levels in worms exposed to a range of sorbitol concentrations overnight. $n = 16$ microplate wells. (G) Number of worms with and without nuclear SKN-1::GFP in the head region observed with confocal microscopy. No SKN-1::GFP was observed in the intestine under any conditions.

nuclear accumulation of SKN-1b/c::GFP, there are also many conditions in which *skn-1*-dependent genes are induced without visible nuclear accumulation (An and Blackwell 2003; Kahn *et al.* 2008; Wu *et al.* 2016). These results are consistent with mechanisms that can increase gene expression via SKN-1 without increasing nuclear levels above what already exists under basal conditions. When accumulation does occur, it is most easily observed in the intestine and epidermis (Wu *et al.* 2016). We used worms expressing a SKN-1b/c::GFP fusion protein to determine if furrow disruption or high osmolarity cause nuclear accumulation of the transcription factor. We counted the number of worms with visible SKN-1b/c::GFP fluorescence when treated with *dpy-7*(*RNAi*), *dpy-10*(*RNAi*), 347 mM sorbitol, or 200 mM NaCl (Figure 6G). We focused on the head epidermis, where *gst-4p*::*GFP* fluorescence is highest in furrow mutants (Figure 5). As shown in Figure 6G, we observed accumulation of SKN-1b/c::GFP only with the positive control prooxidant juglone.

Osmolyte accumulation gene induction is partially dependent on *skn-1*

As mentioned above, our transcriptional analyses show that *skn-1*(*RNAi*) reduced the expression of some osmolyte accumulation genes after exposure to high concentrations of NaCl and in *dpy-7* worms (Figure 4). This represents a novel function for SKN-1. To confirm these effects, we used qPCR and found that *gpdh-1* and *hmit-1.1* expression was partially, or fully, dependent on *skn-1* in worms exposed to 300 mM NaCl
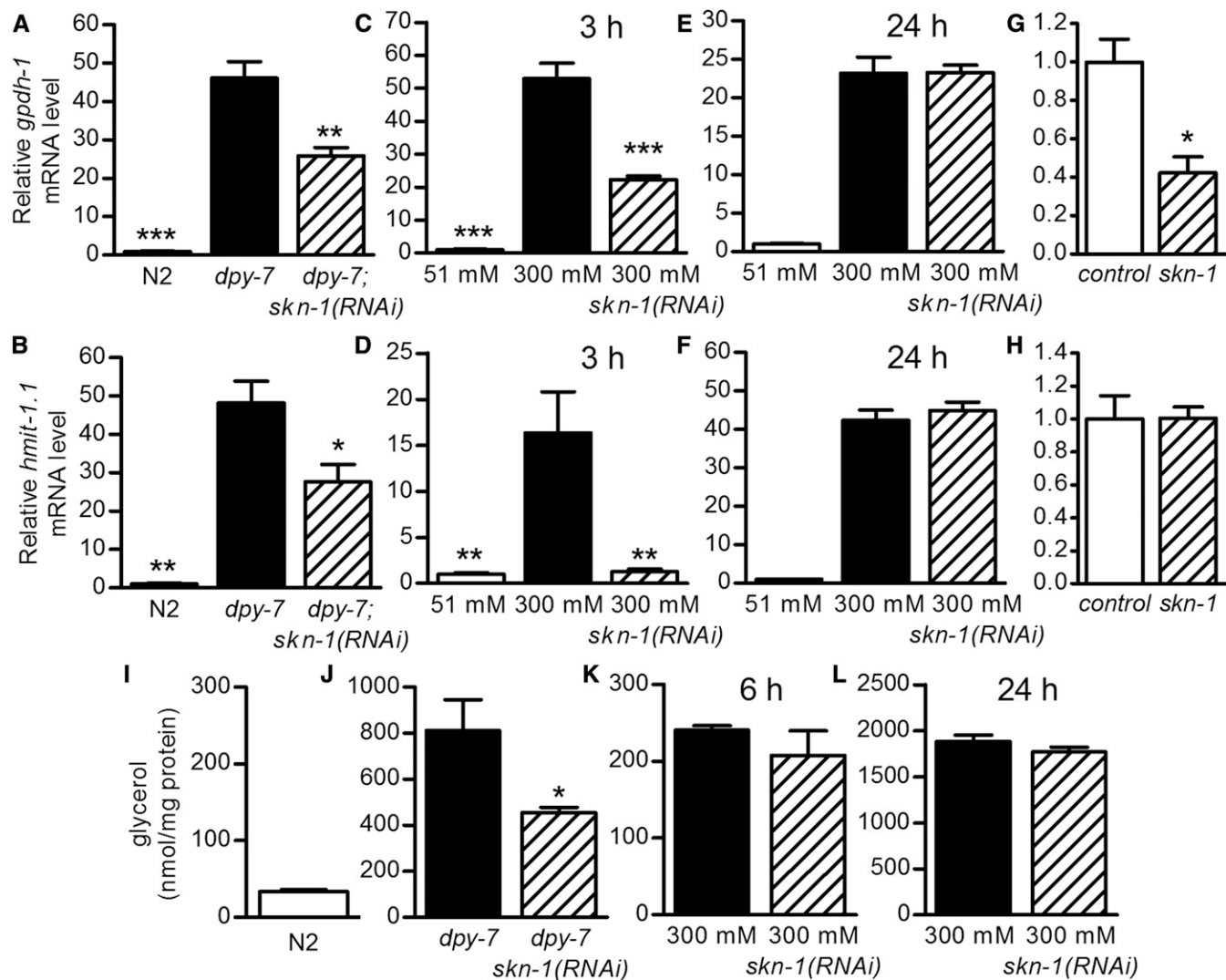
Figure 7 Induction of osmolyte synthesis genes partially requires *skn-1*. (A and B) Relative *gpdh-1* and *hmit-1.1* mRNA levels in *dpy-7(e88)* worms with and without *skn-1(RNAi)*. (C–F) Relative *gpdh-1* and *hmit-1.1* mRNA levels in worms exposed to 300 mM NaCl for 3 hr (C and D) or 24 hr (E and F) with and without *skn-1(RNAi)*. (G and H) Relative *gpdh-1* and *hmit-1.1* mRNA levels in N2 with and without *skn-1(RNAi)* [* $P < 0.05$ *vs. dpy-7* (A and B), 300 mM NaCl (C and D), or control (G and H); $n = 3$–4 replicates of worms]. (I and J) Whole-worm glycerol levels in N2 and *dpy-7(e88)* worms with and without *skn-1(RNAi)*. $n = 7$–9 replicates from two trials. * $P < 0.05$. (K and L) Whole-worm glycerol levels in worms exposed to 300 mM NaCl for 6 (K) or 24 hr (L) with and without *skn-1(RNAi)*. $n = 3$–5 replicates of worms from one trial.

for 3 hr and in *dpy-7* worms (Figure 7, A–D). On the other hand, *skn-1(RNAi)* had no effect on *gpdh-1* or *hmit-1.1* expression after 24 hr on 300 mM NaCl corresponding to a time when glycerol levels approach a steady state (Figure 7, E and F) (Lamitina *et al.* 2004). Under basal conditions in wild-type worms, *gpdh-1*, but not *hmit-1.1*, was partially dependent on *skn-1* (Figure 7, G and H).

We next measured whole-worm glycerol levels in *dpy-7* worms and worms exposed to 300 mM NaCl for 6 or 24 hr, because previous studies reported high glycerol accumulation rates at 6 hr and an elevated steady-state glycerol level at 24 hr (Lamitina *et al.* 2004). As expected, glycerol was dramatically elevated by *dpy-7* mutation and high osmolarity (Figure 7, I–L). Loss of *skn-1* partially reduced glycerol levels in *dpy-7* worms (Figure 7J), but not in worms exposed to high osmolarity

(Figure 7, K and L). Taken together, these data indicate that in worms with disrupted annular furrows, *skn-1* is partially required for the expression of osmotic-responsive genes and accumulation of glycerol. *skn-1* also plays a role in the initial induction of osmolyte accumulation genes by high osmolarity, but without a measurable effect on total glycerol levels.

Physiological assays with skn-1

We next tested if longevity or resistance to a prooxidant was altered in *dpy-10* or *dpy-7* worms as might be expected with constitutive activation of detoxification genes. As shown in Figure 8A, *dpy-7* and *dpy-10* worms had life spans that were very similar to wild-type, and both were actually hypersensitive to the naturally occurring reactive small molecule juglone compared to wild-type worms (Figure S4B in File S1). The
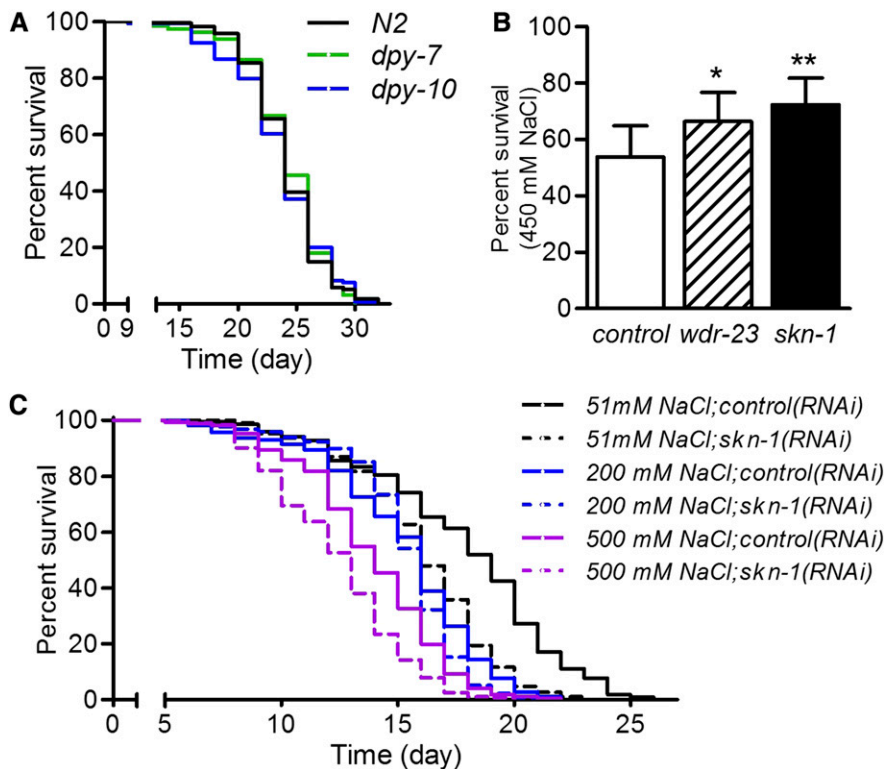
Figure 8 Physiological assays for *skn-1*. (A) Survival curves for longevity. $P > 0.7095$ for *dpy-7* and *dpy-10* relative to N2. $n > 150$ worms from two trials combined. (B) Survival, after 24 hr, of *skn-1* and *wdr-23*(RNAi) worms transferred directly from 51 to 450 mM NaCl agar. ** $P < 0.05$ and ** $P < 0.01$ relative to *control*(RNAi), $n = 4$ trials of 30–581 worms. (C) Survival of chronic exposure to high NaCl. All worms were treated from L1 larval stage except for 500 mM NaCl; these worms were grown on 200 mM NaCl until young adults and then transferred to 500 mM NaCl. $n = 234$–342 worms from three trials. $P < 0.001$ for *skn-1*(RNAi) at 51 and 500 mM NaCl, and $P = 0.0254$ for *skn-1*(RNAi) at 200 mM NaCl.

cuticle is the nematode's primary barrier and its disruption is known to increase sensitivity to diverse small molecules (Partridge *et al.* 2008). The sensitivity of *dpy-7* and *dpy-10* worms is consistent with barrier disruption, and this was also observed for *dpy-5* mutants (Figure S4B in File S1) that do not exhibit an elevated level of *gst* gene expression (Figure 3). Inactivation of *skn-1* further decreased survival (Figure S4B in File S1), consistent with SKN-1 contributing generally to protection against oxidants.

We next conducted experiments to explore the influence of SKN-1 on survival in the presence of high NaCl. We first tested the effects of SKN-1 loss and activation using *skn-1* and *wdr-23*(RNAi), respectively, on the ability of young adult worms to survive for a day after direct transfer from standard growth media containing 51 mM NaCl to media containing 450 mM NaCl. WDR-23 is a direct and robust repressor of SKN-1 (Choe *et al.* 2009). Both *skn-1* and *wdr-23* RNAi increased survival under these conditions, although the effects were small (Figure 8B). These effects suggest that SKN-1 manipulation has complex effects in survival upon acute hyperosmotic exposure that might include compensatory responses.

We also tested the effect of *skn-1*(RNAi) on longevity under conditions of chronic high NaCl. It was recently demonstrated that high NaCl can increase longevity of *C. elegans*, but only in the presence of the DNA synthesis inhibitor 5-fluorodeoxyuridine, which is commonly used to prevent growth of progeny (Anderson *et al.* 2016). To circumvent this complication, we avoided progeny in these experiments by manually transferring adult worms to new plates. Life span was measured at 51 mM NaCl, 200 mM NaCl, and 500 mM NaCl. Worms had to first be

grown on 200 mM NaCl before transferring to 500 mM at the early adult stage to allow larval development. Loss of *skn-1* decreased life span at 500 mM, but this was similar to the effect on standard 51 mM media (Figure 8C), consistent with SKN-1 promoting life span in many contexts.

Distinct, but overlapping, transcription factors function downstream from furrow disruption

Transcriptional control of *gpdh-1* and *nlp-29* upon osmotic challenge in the *C. elegans* epidermis has been reported to be dependent on the ELT-3 GATA transcription factor (Pujol *et al.* 2008b; Rohlfing *et al.* 2010). *nlp-29* also depends on the STAT transcription factor-like protein STA-2 during infection and wounding, but not high NaCl (Dierking *et al.* 2011). ELT-3 has been postulated to cooperate with a number of transcription factors, including SKN-1 and STA-2, to permit stress responses in the epidermis (Block and Shapira 2015). We tested the effects of RNAi for *elt-3*, *sta-2*, and *skn-1* on *gpdh-1*, *gst-4*, and *nlp-29* reporter induction in *dpy-7* furrow mutants (Figure 9). Note that while *gst-4p*::*GFP* and *nlp-29p*::*GFP* are primarily active in the epidermis in this context, *gpdh-1p*::*DsRed2* is active in the intestine and epidermis, and fluorescence levels are from whole worms. RNAi of *skn-1* decreased *gpdh-1p*::*DsRed2* and *gst-4p*::*GFP* confirming a shared requirement; *skn-1*-(RNAi) actually slightly increased *nlp-29p*::*GFP* (Figure 9), which was also observed for *nlp-29* mRNA in RNAseq analysis (Figure S2 in File S1). RNAi of *elt-3* decreased *gst-4p*::*GFP* and *nlp-29p*::*GFP* significantly, but did not have a significant effect on total *gpdh-1p*::*DsRed2* fluorescence (Figure 9). RNAi of *sta-2* decreased *gpdh-1p*::*DsRed2* and *nlp-29p*::*GFP*, but not *gst-*
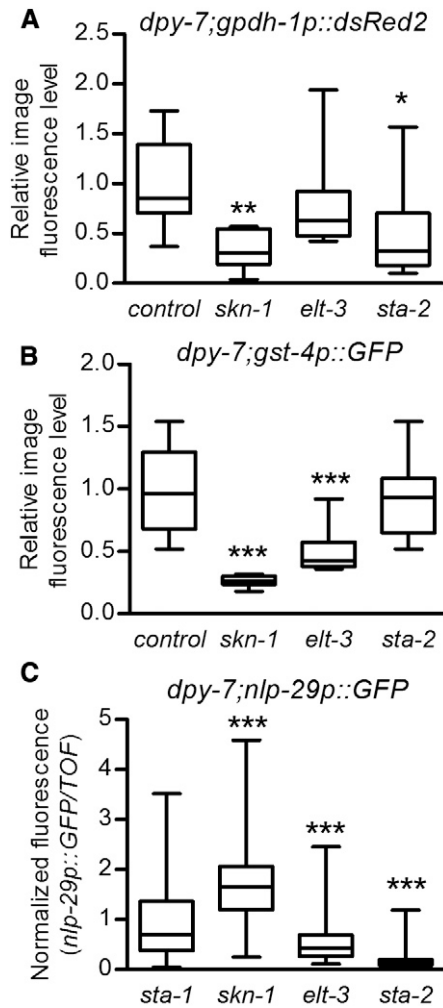
Figure 9 Transcription factor requirements. (A and B) Worms grown to the gravid adult stage were mounted on slides and imaged. Image J was used to measure pixel intensity of individual worms on the GFP (A) or red fluorescent protein RFP (B) filter sets and values were normalized to the mean of *control*(RNAi). *n* = 10 worms. (C) The ratio of *nlp-29p*::*GFP* to time of flight was measured in a BIOSORT and normalized to the negative control *sta-1*(RNAi). *n* = 95–259. Boxes are 25% percentiles above and below the median and whiskers are minimum and maximum. * $P < 0.05$, ** $P < 0.01$, and *** $P < 0.001$ *vs. control*(RNAi).

4p::*GFP*. Using mutants in *dpy-3*, *dpy-7*, and *dpy-10* worms, we confirmed the requirements of *sta-2* and *elt-3* for *nlp-19p*::*GFP* (Figure S4C in File S1). Collectively, the results in Figure 9 and Figure S4 in File S1 suggest that disruption of furrows in the cuticle activates osmotic, detoxification, and antimicrobial transcriptional responses via distinct, but overlapping, downstream transcription factors (Figure 10).

Discussion

Coregulation of three stress responses via cuticle furrows

The cortical layer of the adult *C. elegans* cuticle contains lateral ridges of collagen called alae and circumferential bands called annular furrows. Annular furrows were previously implicated in regulation of *gpdh-1* from a genome-wide RNAi screen (Lamitina *et al.* 2006; Wheeler and Thomas 2006; Choe 2013). Two collagen mutants with furrow defects were also previously shown to have high *nlp-29* expression (Pujol *et al.* 2008b), but it was unknown if other cuticle/epidermal characteristics and stress responses were involved.

Mutation or silencing of six collagen genes (*dpy-2*, *3*, *7*, *8*, *9*, and *10*) severely disrupts furrows without eliminating alae (Cox *et al.* 1980; McMahon *et al.* 2003; Thein *et al.* 2003) (Figure 2 and Table S2). We demonstrate that genetic manipulations that specifically disrupt furrows coactivate osmolyte accumulation, *nlp-29*, and *skn-1*-dependent detoxification genes, but do not activate responses to heat shock, mitochondrial unfolded proteins, or endoplasmic reticulum unfolded proteins (Figure 1, Figure 2, Figure 3, and Figure S2 in File S1). Therefore, our results are consistent with a requirement for annular furrows in regulating osmolyte accumulation, antimicrobial, and *skn-1*-dependent detoxification genes, but not all stress responses.

The cuticle and underlying epidermis form the primary barrier between tissues and the environment, and are therefore well positioned to detect and respond to stress. Recent atomic force microscopy analyses revealed high biomechanical stiffness at furrows relative to annuli (Essmann *et al.* 2017). Nematode body morphology is supported by turgor pressure against the body wall. Hypertonicity-induced water loss depletes turgor pressure in *C. elegans*, and the epidermis and cuticle become physically distorted (Lamitina *et al.* 2004; Choe 2013). Given that furrows are circumferential bands of collagen in the cuticle, we speculate that mechanical strain on these structures likely changes with turgor pressure against the body wall. Physical distortion of furrows or changes in associated extracellular ligand availability could signal via membrane proteins such as integrins, G protein-coupled receptors, phospholipases, enzyme-linked receptors, or ion channels (Clause and Barker 2013; Ross *et al.* 2013; Schiller and Fassler 2013; Gasparski and Beningo 2015). Interestingly, loss of a protein secreted by the epidermis named OSM-11 coactivates osmolyte synthesis, detoxification, and antimicrobial genes (Wheeler and Thomas 2006; Pujol *et al.* 2008b; Dresen *et al.* 2015) without causing any obvious cuticle defects. OSM-11 is thought to act as a ligand for Notch receptors to regulate vulva development and behavior (Komatsu *et al.* 2008; Singh *et al.* 2011). It remains to be seen if Notch signaling plays a role in transmitting signals from the cuticle. It will also be interesting to examine whether hypoosmotic-induced increases in turgor pressure are also able to initiate signals to stress responses.

A G protein-coupled receptor named DCAR-1 is partially required for induction of *nlp-29* in the furrow mutants *dpy-9* and *dpy-10*, but was not required for transcriptional activation of *nlp-29* upon osmotic stress (Zugasti *et al.* 2014). These results suggest that different receptors might be activated downstream from a common furrow-associated sensor.
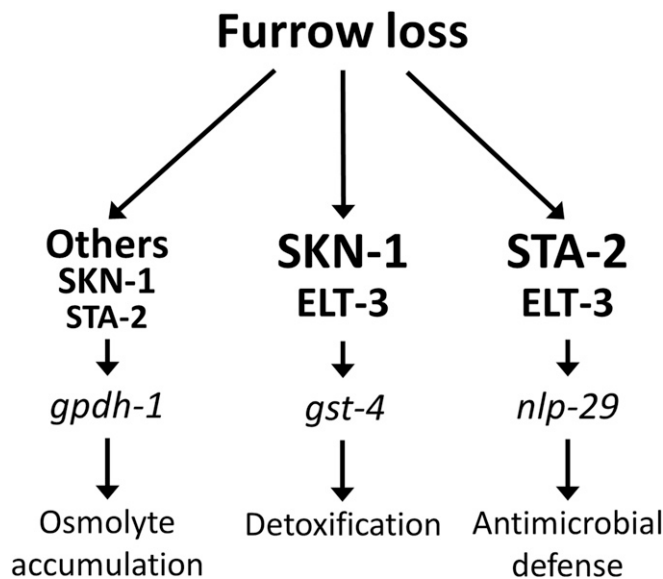
Figure 10 Working model for cuticle annular furrow regulation of stress responses. Disruption of annular furrows in the cuticle initiates signals that are transduced to *nlp-29*, *gpdh-1*, and *gst-4* via different sets of transcription factors.

Distinct transcription factor requirements downstream of furrow disruption

In yeast, at least four transcription factors downstream from an osmosensor-associated protein named HOG1 (hyperosmolarity glycerol response 1) activate downstream genes (Hohmann *et al.* 2007). In mammalian cells, the hypertonicity enhancer-binding protein (TonEBP), also known as NFAT5, regulates a battery of genes responsible for organic osmolyte accumulation and cytoprotection (Lee *et al.* 2011). *C. elegans* lacks a close homolog of TonEBP, and instead GATA transcription factor *elt-3* is at least partially required for *gpdh-1* and *nlp-29* induction by high NaCl in the epidermis (Pujol *et al.* 2008b; Rohlfing *et al.* 2010).

Our results are consistent with distinct, but partially overlapping, transcriptional pathways functioning downstream from furrow loss to activate distinct stress responses (Figure 10). Interestingly, *elt-3*, in addition to *skn-1*, is required for the detoxification response to furrow loss (Figure 9). Similarly, *elt-3* and *skn-1* were recently shown to coregulate detoxification genes in a stress-sensitive mutant (Hu *et al.* 2017). Conversely, *sta-2* is completely required and *elt-3* is partially required for the antimicrobial response in the epidermis (Figure 9 and Figure S4B in File S1). We found evidence of a novel role for *skn-1* in induction of *gpdh-1* (Figure 7 and Figure 9). SKN-1-binding elements were previously defined (Blackwell *et al.* 1994; Rupert *et al.* 1998), but we found none within 3-kb upstream of *gpdh-1* nor *hmit-1.1* start codons, suggesting indirect regulation.

SKN-1-dependent gene induction

Regulation of intracellular SKN-1/Nrf signaling in response to reactive small molecules is well studied in mammalian cells and *C. elegans* (Taguchi *et al.* 2011; Niture *et al.* 2013; Blackwell *et al.* 2015; Wu *et al.* 2016, 2017). Conversely, very little is known about regulation of SKN-1/Nrf pathways via the ECM. A lack of obvious increases in nuclear accumulation (Figure 6G) is consistent with regulation by post-translational modification or by changes in interaction with DNA or cofactors.

Antioxidant/detoxification pathways protect tissues from inflammation and fibrosis, making coordination of Nrf2 signaling and the ECM important to disease pathogenesis (Wu *et al.* 2015; Ahmed *et al.* 2017; Xu *et al.* 2017). In cultured mammalian vascular cells, Nrf2-dependent responses have been shown to be activated by mechanical shear stress that models turbulent blood flow, with intracellular reactive oxygen species (ROS) being implicated as a downstream signal (Jones *et al.* 2007; Warabi *et al.* 2007; Hsieh *et al.* 2014). It is not known how the extracellular mechanical stimulus is detected and transduced into the cell where ROS are generated. It was recently shown that a *skn-1*-dependent detoxification response could be activated by an increase in ROS at the ER via sulfenylation of the kinase IRE-1 (Hourihan *et al.* 2016). It remains to be seen if ROS are increased in furrow mutants through the action of an endogenous enzyme. Signaling mechanisms that act downstream of annular furrow disruption to activate SKN-1-mediated transcriptional responses will define a novel mode of signaling for this conserved family of stress and longevity factors.

Literature Cited

Ahmed, S. M., L. Luo, A. Namani, X. J. Wang, and X. Tang, 2017 Nrf2 signaling pathway: pivotal roles in inflammation. Biochim. Biophys. Acta 1863: 585–597. https://doi.org/10.1016/j.bbadis.2016.11.005

Alvarez, L. I., M. L. Mottier, and C. E. Lanusse, 2007 Drug transfer into target helminth parasites. Trends Parasitol. 23: 97–104. https://doi.org/10.1016/j.pt.2007.01.003

An, J. H., and T. K. Blackwell, 2003 SKN-1 links *C. elegans* mesendodermal specification to a conserved oxidative stress response. Genes Dev. 17: 1882–1893. https://doi.org/10.1101/gad.1107803

Anderson, E. N., M. E. Corkins, J. C. Li, K. Singh, S. Parsons *et al.*, 2016 *C. elegans* lifespan extension by osmotic stress requires FUdR, base excision repair, FOXO, and sirtuins. Mech. Ageing Dev. 154: 30–42. https://doi.org/10.1016/j.mad.2016.01.004

Blackwell, T. K., B. Bowerman, J. R. Priess, and H. Weintraub, 1994 Formation of a monomeric DNA binding domain by SKN-1 bZIP and homeodomain elements. Science 266: 621–628. https://doi.org/10.1126/science.7939715

Blackwell, T. K., M. J. Steinbaugh, J. M. Hourihan, C. Y. Ewald, and M. Isik, 2015 SKN-1/Nrf, stress responses, and aging in *Caenorhabditis elegans*. Free Radic. Biol. Med. 88: 290–301. https://doi.org/10.1016/j.freeradbiomed.2015.06.008

Block, D. H., and M. Shapira, 2012 GATA transcription factors as tissue-specific master regulators for induced responses. Worm. 4 (4):e1118607. https://doi.org/10.1080/21624054.2015.1118607

Brenner, S., 1974 The genetics of *Caenorhabditis elegans*. Genetics 77: 71–94.

Bryan, H. K., A. Olayanju, C. E. Goldring, and B. K. Park, 2013 The Nrf2 cell defence pathway: Keap1-dependent and -independent mechanisms of regulation. Biochem. Pharmacol. 85: 705–717. https://doi.org/10.1016/j.bcp.2012.11.016

Burns, A. R., I. M. Wallace, J. Wildenhain, M. Tyers, G. Giaever *et al.*, 2010 A predictive model for drug bioaccumulation and bioactivity in *Caenorhabditis elegans*. Nat. Chem. Biol. 6: 549–557. https://doi.org/10.1038/nchembio.380

Chisholm, A. D., and S. Xu, 2012 The *Caenorhabditis elegans* epidermis as a model skin. II: differentiation and physiological roles. Wiley Interdiscip. Rev. Dev. Biol. 1: 879–902. https://doi.org/10.1002/wdev.77

Choe, K. P., 2013 Physiological and molecular mechanisms of salt and water homeostasis in the nematode *Caenorhabditis elegans*. Am. J. Physiol. Regul. Integr. Comp. Physiol. 305: R175–R186. https://doi.org/10.1152/ajpregu.00109.2013

Choe, K. P., A. J. Przybysz, and K. Strange, 2009 The WD40 repeat protein WDR-23 functions with the CUL4/DDB1 ubiquitin ligase to regulate nuclear abundance and activity of SKN-1 in *Caenorhabditis elegans*. Mol. Cell. Biol. 29: 2704–2715. https://doi.org/10.1128/MCB.01811-08

Choe, K. P., C. K. Leung, and M. M. Miyamoto, 2012 Unique structure and regulation of the nematode detoxification gene regulator, SKN-1: implications to understanding and controlling drug resistance. Drug Metab. Rev. 44: 209–223. https://doi.org/10.3109/03602532.2012.684799

Clause, K. C., and T. H. Barker, 2013 Extracellular matrix signaling in morphogenesis and repair. Curr. Opin. Biotechnol. 24: 830–833. https://doi.org/10.1016/j.copbio.2013.04.011

Cox, G. N., J. S. Laufer, M. Kusch, and R. S. Edgar, 1980 Genetic and phenotypic characterization of roller mutants of *Caenorhabditis elegans*. Genetics 95: 317–339.

Dierking, K., J. Polanowska, S. Omi, I. Engelmann, M. Gut *et al.*, 2011 Unusual regulation of a STAT protein by an SLC6 family transporter in C. elegans epidermal innate immunity. Cell Host Microbe 9: 425–435. https://doi.org/10.1016/j.chom.2011.04.011

Dresen, A., S. Finkbeiner, M. Dottermusch, J. S. Beume, Y. Li *et al.*, 2015 *Caenorhabditis elegans* OSM-11 signaling regulates SKN-1/Nrf during embryonic development and adult longevity and stress response. Dev. Biol. 400: 118–131. https://doi.org/10.1016/j.ydbio.2015.01.021

Essmann, C. L., M. Elmi, M. Shaw, G. M. Anand, V. M. Pawar *et al.*, 2017 In-vivo high resolution AFM topographic imaging of *Caenorhabditis elegans* reveals previously unreported surface structures of cuticle mutants. Nanomedicine 13: 183–189. https://doi.org/10.1016/j.nano.2016.09.006

Gaggar, A., and N. Weathington, 2016 Bioactive extracellular matrix fragments in lung health and disease. J. Clin. Invest. 126: 3176–3184. https://doi.org/10.1172/JCI83147

Gasparski, A. N., and K. A. Beningo, 2015 Mechanoreception at the cell membrane: more than the integrins. Arch. Biochem. Biophys. 586: 20–26. https://doi.org/10.1016/j.abb.2015.07.017

Hay, E. D., 1981 Extracellular matrix. J. Cell Biol. 91: 205s–223s. https://doi.org/10.1083/jcb.91.3.205s

Hobert, O., 2002 PCR fusion-based approach to create reporter gene constructs for expression analysis in transgenic *C. elegans*. Biotechniques 32: 728–730.

Hohmann, S., M. Krantz, and B. Nordlander, 2007 Yeast osmoregulation. Methods Enzymol. 428: 29–45. https://doi.org/10.1016/S0076-6879(07)28002-4

Hourihan, J. M., L. E. Moronetti Mazzeo, L. P. Fernandez-Cardenas, and T. K. Blackwell, 2016 Cysteine sulfenylation directs IRE-1 to activate the SKN-1/Nrf2 antioxidant response. Mol. Cell 63: 553–566. https://doi.org/10.1016/j.molcel.2016.07.019

Hsieh, H. J., C. A. Liu, B. Huang, A. H. Tseng, and D. L. Wang, 2014 Shear-induced endothelial mechanotransduction: the interplay between reactive oxygen species (ROS) and nitric oxide (NO) and the pathophysiological implications. J. Biomed. Sci. 21: 3. https://doi.org/10.1186/1423-0127-21-3

Hu, Q., D. R. D'Amora, L. T. MacNeil, A. J. M. Walhout, and T. J. Kubiseski, 2017 The oxidative stress response in Caenorhabditis elegans requires the GATA transcription factor ELT-3 and SKN-1/Nrf2. Genetics 206: 1909–1922.

Hu, R., C. Xu, G. Shen, M. R. Jain, T. O. Khor *et al.*, 2006 Identification of Nrf2-regulated genes induced by chemopreventive isothiocyanate PEITC by oligonucleotide microarray. Life Sci. 79: 1944–1955. https://doi.org/10.1016/j.lfs.2006.06.019

Huang, D. W., B. T. Sherman, and R. A. Lempicki, 2009 Systematic and integrative analysis of large gene lists using DAVID bioinformatics resources. Nat. Protoc. 4: 44–57. https://doi.org/10.1038/nprot.2008.211

Johnstone, I. L., 2000 Cuticle collagen genes. Expression in *Caenorhabditis elegans*. Trends Genet. 16: 21–27. https://doi.org/10.1016/S0168-9525(99)01857-0

Jones, C. I., III, H. Zhu, S. F. Martin, Z. Han, Y. Li *et al.*, 2007 Regulation of antioxidants and phase 2 enzymes by shear-induced reactive oxygen species in endothelial cells. Ann. Biomed. Eng. 35: 683–693. https://doi.org/10.1007/s10439-007-9279-9

Jones, D., D. K. Dixon, R. W. Graham, and E. P. Candido, 1989 Differential regulation of closely related members of the hsp16 gene family in *Caenorhabditis elegans*. DNA 8: 481–490. https://doi.org/10.1089/dna.1.1989.8.481

Kage-Nakadai, E., T. Uehara, and S. Mitani, 2011 H+/myo-inositol transporter genes, *hmit-1.1* and *hmit-1.2*, have roles in the osmoprotective response in *Caenorhabditis elegans*. Biochem. Biophys. Res. Commun. 410: 471–477. https://doi.org/10.1016/j.bbrc.2011.06.001

Kahn, N. W., S. L. Rea, S. Moyle, A. Kell, and T. E. Johnson, 2008 Proteasomal dysfunction activates the transcription factor SKN-1 and produces a selective oxidative-stress response in *Caenorhabditis elegans*. Biochem. J. 409: 205–213. https://doi.org/10.1042/BJ20070521

Kamath, R. S., M. Martinez-Campos, P. Zipperlen, A. G. Fraser, and J. Ahringer, 2001 Effectiveness of specific RNA-mediated interference through ingested double-stranded RNA in *Caenorhabditis elegans*. Genome Biol. 2: RESEARCH0002.

Kamath, R. S., A. G. Fraser, Y. Dong, G. Poulin, R. Durbin *et al.*, 2003 Systematic functional analysis of the *Caenorhabditis elegans* genome using RNAi. Nature 421: 231–237. https://doi.org/10.1038/nature01278

Kell, A., N. Ventura, N. Kahn, and T. E. Johnson, 2007 Activation of SKN-1 by novel kinases in *Caenorhabditis elegans*. Free Radic. Biol. Med. 43: 1560–1566. https://doi.org/10.1016/j.freeradbiomed.2007.08.025

Ko, F. C., and K. L. Chow, 2002   A novel thioredoxin-like protein encoded by the *C. elegans dpy-11* gene is required for body and sensory organ morphogenesis. Development 129: 1185–1194.

Komatsu, H., M. Y. Chao, J. Larkins-Ford, M. E. Corkins, G. A. Somers *et al.*, 2008   OSM-11 facilitates LIN-12 Notch signaling during *Caenorhabditis elegans* vulval development. PLoS Biol. 6: e196. https://doi.org/10.1371/journal.pbio.0060196

Lamitina, S. T., R. Morrison, G. W. Moeckel, and K. Strange, 2004   Adaptation of the nematode *Caenorhabditis elegans* to extreme osmotic stress. Am. J. Physiol. Cell Physiol. 286: C785–C791. https://doi.org/10.1152/ajpcell.00381.2003

Lamitina, T., C. G. Huang, and K. Strange, 2006   Genome-wide RNAi screening identifies protein damage as a regulator of osmoprotective gene expression. Proc. Natl. Acad. Sci. USA 103: 12173–12178. https://doi.org/10.1073/pnas.0602987103

Lee, K. Z., M. Kniazeva, M. Han, N. Pujol, and J. J. Ewbank, 2010   The fatty acid synthase fasn-1 acts upstream of WNK and Ste20/GCK-VI kinases to modulate antimicrobial peptide expression in *C. elegans* epidermis. Virulence 1: 113–122. https://doi.org/10.4161/viru.1.3.10974

Lee, S. D., S. Y. Choi, S. W. Lim, S. T. Lamitina, S. N. Ho *et al.*, 2011   TonEBP stimulates multiple cellular pathways for adaptation to hypertonic stress: organic osmolyte-dependent and -independent pathways. Am. J. Physiol. Renal Physiol. 300: F707–F715. https://doi.org/10.1152/ajprenal.00227.2010

Leung, C. K., A. Deonarine, K. Strange, and K. P. Choe, 2011   High-throughput screening and biosensing with fluorescent *C. elegans* strains. J. Vis. Exp. 51: 2745.

McMahon, L., J. M. Muriel, B. Roberts, M. Quinn, and I. L. Johnstone, 2003   Two sets of interacting collagens form functionally distinct substructures within a *Caenorhabditis elegans* extracellular matrix. Mol. Biol. Cell 14: 1366–1378. https://doi.org/10.1091/mbc.E02-08-0479

Niture, S. K., R. Khatri, and A. K. Jaiswal, 2014   Regulation of Nrf2-an update. Free Radic. Biol. Med. 66: 36–44. https://doi.org/10.1016/j.freeradbiomed.2013.02.008

Oliveira, R. P., J. P. Abate, K. Dilks, J. Landis, J. Ashraf *et al.*, 2009   Condition-adapted stress and longevity gene regulation by *Caenorhabditis elegans* SKN-1/Nrf. Aging Cell 8: 524–541. https://doi.org/10.1111/j.1474-9726.2009.00501.x

Page, A. P., and I. L. Johnstone, 2007   The cuticle (March 19, 2007), *WormBook*, ed. The. C. *elegans* Research Community, WormBook, doi/10.1895/wormbook.1.138.1, http://www.wormbook.org. https://doi.org/doi/10.1895/wormbook.1.138.1

Park, S.-K., P. M. Tedesco, and T. E. Johnson, 2009   Oxidative stress and longevity in *Caenorhabditis elegans* as mediated by SKN-1. Aging Cell 8: 258–269. https://doi.org/10.1111/j.1474-9726.2009.00473.x

Partridge, F. A., A. W. Tearle, M. J. Gravato-Nobre, W. R. Schafer, and J. Hodgkin, 2008   The *C. elegans* glycosyltransferase BUS-8 has two distinct and essential roles in epidermal morphogenesis. Dev. Biol. 317: 549–559. https://doi.org/10.1016/j.ydbio.2008.02.060

Pimentel, H., N. L. Bray, S. Puente, P. Melsted, and L. Pachter, 2017   Differential analysis of RNA-seq incorporating quantification uncertainty. Nat. Methods 14: 687–690. https://doi.org/10.1038/nmeth.4324

Pujol, N., S. Cypowyj, K. Ziegler, A. Millet, A. Astrain *et al.*, 2008a   Distinct innate immune responses to infection and wounding in the *C. elegans* epidermis. Curr. Biol. 18: 481–489. https://doi.org/10.1016/j.cub.2008.02.079

Pujol, N., O. Zugasti, D. Wong, C. Couillault, C. L. Kurz *et al.*, 2008b   Anti-fungal innate immunity in *C. elegans* is enhanced by evolutionary diversification of antimicrobial peptides. PLoS Pathog. 4: e1000105. https://doi.org/10.1371/journal.ppat.1000105

Rohlfing, A. K., Y. Miteva, S. Hannenhalli, and T. Lamitina, 2010   Genetic and physiological activation of osmosensitive gene expression mimics transcriptional signatures of pathogen infection in *C. elegans*. PLoS One 5: e9010. https://doi.org/10.1371/journal.pone.0009010

Rohlfing, A. K., Y. Miteva, L. Moronetti, L. He, and T. Lamitina, 2011   The *Caenorhabditis elegans* mucin-like protein OSM-8 negatively regulates osmosensitive physiology via the transmembrane protein PTR-23. PLoS Genet. 7: e1001267. https://doi.org/10.1371/journal.pgen.1001267

Ross, T. D., B. G. Coon, S. Yun, N. Baeyens, K. Tanaka *et al.*, 2013   Integrins in mechanotransduction. Curr. Opin. Cell Biol. 25: 613–618. https://doi.org/10.1016/j.ceb.2013.05.006

Rozario, T., and D. W. DeSimone, 2010   The extracellular matrix in development and morphogenesis: a dynamic view. Dev. Biol. 341: 126–140. https://doi.org/10.1016/j.ydbio.2009.10.026

Rual, J. F., J. Ceron, J. Koreth, T. Hao, A. S. Nicot *et al.*, 2004   Toward improving *Caenorhabditis elegans* phenome mapping with an ORFeome-based RNAi library. Genome Res. 14: 2162–2168. https://doi.org/10.1101/gr.2505604

Rupert, P. B., G. W. Daughdrill, B. Bowerman, and B. W. Matthews, 1998   A new DNA-binding motif in the Skn-1 binding domain-DNA complex. Nat. Struct. Biol. 5: 484–491. https://doi.org/10.1038/nsb0698-484

Samarakoon, R., J. M. Overstreet, and P. J. Higgins, 2013   TGF-beta signaling in tissue fibrosis: redox controls, target genes and therapeutic opportunities. Cell. Signal. 25: 264–268. https://doi.org/10.1016/j.cellsig.2012.10.003

Schiller, H. B., and R. Fassler, 2013   Mechanosensitivity and compositional dynamics of cell-matrix adhesions. EMBO Rep. 14: 509–519. https://doi.org/10.1038/embor.2013.49

Shen, X., R. E. Ellis, K. Lee, C. Y. Liu, K. Yang *et al.*, 2001   Complementary signaling pathways regulate the unfolded protein response and are required for *C. elegans* development. Cell 107: 893–903. https://doi.org/10.1016/S0092-8674(01)00612-2

Singh, K., M. Y. Chao, G. A. Somers, H. Komatsu, M. E. Corkins *et al.*, 2011   *C. elegans* Notch signaling regulates adult chemosensory response and larval molting quiescence. Curr. Biol. 21: 825–834. https://doi.org/10.1016/j.cub.2011.04.010

Steinbaugh, M. J., S. D. Narasimhan, S. Robida-Stubbs, L. E. Moronetti Mazzeo, J. M. Dreyfuss *et al.*, 2015   Lipid-mediated regulation of SKN-1/Nrf in response to germ cell absence. Elife 4: 07836. https://doi.org/10.7554/eLife.07836

Sykiotis, G., and D. Bohmann, 2010   Stress-activated cap'n'collar transcription factors in aging and human disease. Sci. Signal. 3: re3. https://doi.org/10.1126/scisignal.3112re3

Taffoni, C., and N. Pujol, 2015   Mechanisms of innate immunity in *C. elegans* epidermis. Tissue Barriers 3: e1078432. https://doi.org/10.1080/21688370.2015.1078432

Taguchi, K., H. Motohashi, and M. Yamamoto, 2011   Molecular mechanisms of the Keap1-Nrf2 pathway in stress response and cancer evolution. Genes Cells 16: 123–140. https://doi.org/10.1111/j.1365-2443.2010.01473.x

Tang, L., and K. P. Choe, 2015   Characterization of *skn-1/wdr-23* phenotypes in *Caenorhabditis elegans*; pleiotrophy, aging, glutathione, and interactions with other longevity pathways. Mech. Ageing Dev. 149: 88–98. https://doi.org/10.1016/j.mad.2015.06.001

Thakur, N., N. Pujol, L. Tichit, and J. J. Ewbank, 2014   Clone mapper: an online suite of tools for RNAi experiments in *Caenorhabditis elegans*. G3 (Bethesda) 4: 2137–2145. https://doi.org/10.1534/g3.114.013052

Thein, M. C., G. McCormack, A. D. Winter, I. L. Johnstone, C. B. Shoemaker *et al.*, 2003   *Caenorhabditis elegans* exoskeleton collagen COL-19: an adult-specific marker for collagen modification and assembly, and the analysis of organismal morphology. Dev. Dyn. 226: 523–539. https://doi.org/10.1002/dvdy.10259

Tong, A., G. Lynn, V. Ngo, D. Wong, S. L. Moseley *et al.*, 2009   Negative regulation of *Caenorhabditis elegans* epidermal damage responses by death-associated protein kinase. Proc. Natl. Acad. Sci. USA 106: 1457–1461. https://doi.org/10.1073/pnas.0809339106

Warabi, E., W. Takabe, T. Minami, K. Inoue, K. Itoh *et al.*, 2007   Shear stress stabilizes NF-E2-related factor 2 and induces antioxidant genes in endothelial cells: role of reactive oxygen/nitrogen species. Free Radic. Biol. Med. 42: 260–269. https://doi.org/10.1016/j.freeradbiomed.2006.10.043

Ward, J. D., B. Mullaney, B. J. Schiller, L. D. He, S. E. Petnic *et al.*, 2014   Defects in the *C. elegans* acyl-CoA synthase, acs-3, and nuclear hormone receptor, nhr-25, cause sensitivity to distinct, but overlapping stresses. PLoS One 9: e92552. https://doi.org/10.1371/journal.pone.0092552

Wheeler, J. M., and J. H. Thomas, 2006   Identification of a novel gene family involved in osmotic stress response in *Caenorhabditis elegans*. Genetics 174: 1327–1336. https://doi.org/10.1534/genetics.106.059089

Winograd-Katz, S. E., R. Fassler, B. Geiger, and K. R. Legate, 2014   The integrin adhesome: from genes and proteins to human disease. Nat. Rev. Mol. Cell Biol. 15: 273–288. https://doi.org/10.1038/nrm3769

Wu, C. W., A. Deonarine, A. Przybysz, K. Strange, and K. P. Choe, 2016   The Skp1 homologs SKR-1/2 are required for the Caenorhabditis elegans SKN-1 antioxidant/detoxification response independently of p38 MAPK. PLoS Genet. 12: e1006361. https://doi.org/10.1371/journal.pgen.1006361

Wu, C. W., Y. Wang, and K. P. Choe, 2017   F-box protein XREP-4 Is a new regulator of the oxidative stress response in *Caenorhabditis elegans*. Genetics 206: 859–871. https://doi.org/10.1534/genetics.117.200592

Wu, H., L. Kong, Y. Cheng, Z. Zhang, Y. Wang *et al.*, 2015   Metallothionein plays a prominent role in the prevention of diabetic nephropathy by sulforaphane via up-regulation of Nrf2. Free Radic. Biol. Med. 89: 431–442 (corrigenda: Free Radic. Biol. Med. 97: 621). https://doi.org/10.1016/j.freeradbiomed.2015.08.009

Xu, Y., W. Tai, X. Qu, W. Wu, Z. Li *et al.*, 2017   Rapamycin protects against paraquat-induced pulmonary fibrosis: activation of Nrf2 signaling pathway. Biochem. Biophys. Res. Commun. 490: 535–540. https://doi.org/10.1016/j.bbrc.2017.06.074

Yoneda, T., C. Benedetti, F. Urano, S. G. Clark, H. P. Harding *et al.*, 2004   Compartment-specific perturbation of protein handling activates genes encoding mitochondrial chaperones. J. Cell Sci. 117: 4055–4066. https://doi.org/10.1242/jcs.01275

Zugasti, O., N. Bose, B. Squiban, J. Belougne, C. L. Kurz *et al.*, 2014   Activation of a G protein-coupled receptor by its endogenous ligand triggers the innate immune response of *Caenorhabditis elegans*. Nat. Immunol. 15: 833–838. https://doi.org/10.1038/ni.2957

Zugasti, O., N. Thakur, J. Belougne, B. Squiban, C. L. Kurz *et al.*, 2016   A quantitative genome-wide RNAi screen in *C. elegans* for antifungal innate immunity genes. BMC Biol. 14: 35. https://doi.org/10.1186/s12915-016-0256-3

Communicating editor: B. Goldstein